International Journal of Heat and Mass Transfer 64 (2013) 1031–1040

Contents lists available at SciVerse ScienceDirect

International Journal of Heat and Mass Transfer

journal homepage: www.elsevier.com/locate/ijhmt

Analysis of the effect of stent emplacement on LDL transport within an artery

Shujuan Wang, Kambiz Vafai *

Department of Mechanical Engineering, University of California, Riverside 92521, CA, United States

ARTICLE INFO

Article history:
Received 22 February 2013
Received in revised form 4 May 2013
Accepted 15 May 2013

Keywords:
Low-density lipoprotein transport
Stent
Arterial wall
Porous media

ABSTRACT

A comprehensive analytical solution for macromolecule transport within an artery is presented. The arterial wall is modeled as a multilayer structure to accommodate the homogeneous layers within it. The arterial layers and the stent are treated as porous media to accommodate transport across the complex wall structure. The volume-averaged transport equations and the method of matched asymptotic expansions are employed to solve for species concentration distributions within the stent and various layers of the arterial wall. The analytical results are found to be in very good agreement with the numerical results. The effect of stent compactness on LDL concentration along the lumen flow direction as well across the different layers is investigated. This work provides essential fundamental information for macromolecular transport within an artery with or without the presence of a stent.

© 2013 Elsevier Ltd. All rights reserved.

1. Introduction

Cardiovascular diseases (CVD) have been the subject of various studies. The American Heart Association [1] reports that the number of American adults with CVD is close to 80 million. One out of 2.8 persons expires due to a cardiovascular disease. A major contributor of CVD, atherosclerosis is caused by the abnormal accumulation of macromolecules, such as lipoprotein, within the arterial wall.

Insertion of a stent within an affected vessel is one of the prevalent medical treatments for alleviating an arterial stenosis while maintaining the stability of the vessel. Stents, which are small metallic tubes, are inserted within an artery to open up the arterial stenosis and maintain the structural stability. Self-expanding stent is the preliminary design made by alloys, such as Nitinol, with shape characteristics. The stent is compressed into a catheter and then expelled from it at the treatment site (Stoeckel et al. 2004 [2]). In the early 1980s, the stent was redesigned to be expandable by an angioplasty balloon [3]. After expansion, the stent stuck to the arterial wall as a latticed structure.

The arterial models constitute three major categories [4,5], namely, wall-free, lumen-wall, and multi-layer-wall models. These models are applied for the analysis of macromolecule transport within an arterial wall (Pappitsch and Pertold [6]; Wada and Karino [7]; Moore and Ethier [8]; Stangeby and Ethier [9,10]; Ai and Vafai [11]). The wall-free model represents the arterial wall by a set of boundary conditions [12] while the lumen-wall model assumes the wall to be a homogeneous layer. The most comprehensive representation is the multi-layer-wall model [13–15], which divides the arterial wall into several heterogeneous porous layers, namely endothelium, intima, internal elastic (IEL) and media layers. The multilayer model presents different attributes within each arterial layer. As such it is considered to be the most realistic model. The presence of a stent with a latticed structure is also modeled as a porous medium with a specific permeability and an effective diffusivity.

Several models are used to describe the fluid flow in a porous medium, such as Darcy, Darcy–Forchheimer, and Brinkman models. The flow velocity is linearly related to the pressure across the porous medium in the classic Darcy model. Darcy–Forchheimer model adds a Forchheimer term, which represents the inertial effects. Brinkman model incorporates the effect of solid boundaries on the porous medium. With respect to the mass transport within the arterial wall, the volume-averaged convection–diffusion-reaction equation is applied within the intima and media, coupled with Staverman–Kedem–Katchalsky equations in the endothelium and IEL [5]. Since the Staverman–Kedem–Katchalsky equations do not take into account the transient and boundary conditions, their application is limited. Yang and Vafai [5] have modeled the transport within the four layers of the arterial wall by incorporating the Staverman filtration and osmotic reflection coefficients within the volume averaged porous media equations. This alleviates the disadvantages of Staverman–Kedem–Katchalsky equations.

The lumen in the artery is mainly composed of blood cells and plasma. The blood can be considered to be a two-phase system, i.e.,

* Corresponding author.
E-mail address: Vafai@ENGR.UCR.EDU (K. Vafai).

0017-9310/$ - see front matter © 2013 Elsevier Ltd. All rights reserved.
http://dx.doi.org/10.1016/j.ijheatmasstransfer.2013.05.041

Nomenclature

c	LDL concentration [mol/m^3]
Da	Darcy number
D	LDL diffusivity [m^2/s]
F	dimensionless inertia coefficient
H^*	thickness of the layers [m]
k	reaction coefficient [s^{-1}]
K	permeability [m^2]
L	length of the artery [m]
L_{end}	thickness of the endothelium layer [m]
N	non-dimensional concentration
u_{ch}	characteristic velocity [m/s]
Δp	pressure drop across arterial wall [Pa]
Re_{ch}	Reynolds number $= (u_{ch}\sqrt{K})/v_f$
Sc	Schmidt number
$U_{0,i}$	streamwise velocity at the ith interface [m/s]
R_{Cell}	radius of the endothelial cell [m]
R	radius of the lumen domain [m]
σ_f	the Stavernan filtration coefficient
$\mathbf{V}$	velocity vector [m/s]
p	hydraulic pressure [Pa]
U	maximum velocity at the entrance [m/s]
ε	gauge parameter
v	filtration velocity [m/s]
δ	porosity
μ	dynamic viscosity [kg/(m s)]
ξ	non-dimensional axial location
η	non-dimensional radial location
ρ	fluid density [kg/m^3]
u	axial velocity [m/s]

Symbol

$\langle\rangle$	local volume average

Subscripts

ch	characteristic
f	fluid
i	i = 0, 1, 2, 3 and 4 representing lumen, endothelium, intima, IEL, and media, respectively
70 mmHg	refers to properties with a gauge pressure of 70 mmHg
eff	refers to an effective property
end	refers to the endothelium layer
m	normal coordinate

the cells and the plasma. The blood cells could affect the flow field within the small size vessels. As such, the blood can exhibit non-Newtonian behavior in the small size vessels. The viscosity of the blood as a non-Newtonian fluid can be expressed by several models [16–18]. However, for large and medium arteries, it is generally reasonable to consider the blood as a Newtonian fluid.

In the present study, the fluid flow and mass transfer within an arterial wall is analyzed using a four-layer model which is a modification of Khakpour and Vafai [19] and Yang and Vafai's works [5]. A comprehensive analytical solution of the low-density lipoprotein (LDL) transport in the arterial wall is presented. The analytical solution of the LDL transport in the arterial wall with a stent is obtained and compared with the corresponding numerical solution. Furthermore, the effect of stent compactness on the LDL concentration distribution is also shown.

2. Analysis

2.1. Wall model

Fig. 1[a] shows the typical anatomical structure of an arterial wall discussed by Yang and Vafai [5]. It is composed of five layers, i.e. glycocalyx, endothelium, internal elastic lamina, media and adventitia. Since its average thickness is only 60 nm, the glycocalyx is generally not considered in the model (Michel and Curry [20]; Tarbell [21]). Endothelium, a layer of cells interconnected with intercellular junctions is considered followed by IEL, which is composed of an impermeable elastic tissue with fenestral pores. The intima consists of proteoglycan and collagen fibers and the media layer contains smooth muscle cells and elastic connective tissue, comprised of lymphatic and vasa vasorum, is loosely connected to the adventitia. The thickness and properties of each layer is shown in Table 1 [5,22,23].

2.2. Governing equations

Fig. 1(b) shows the arterial wall representation with four different macroscopically homogeneous porous layers. The lumen is assumed to be Newtonian and incompressible with constant properties. The momentum and mass transport equations in the lumen are:

$$\begin{aligned} &\nabla\cdot\mathbf{V}=0\\ &\rho\frac{D\mathbf{V}}{Dt}=-\nabla p+\mu_f\nabla^2\mathbf{V}\\ &\frac{\partial c}{\partial t}+\mathbf{V}\cdot\nabla c=D\nabla^2 c \end{aligned} \tag{1}$$

where $\mathbf{V}$ is the velocity vector, c LDL concentration, p hydraulic pressure and ρ, μ_f, and D are the fluid density, viscosity, and diffusivity respectively.

According to the Darcy numbers in Table 1, the viscosity effect for this problem needs to be considered. However, Darcy's model cannot describe the viscosity and inertia effects. The volume-averaged equations with viscosity and Forchheimer terms are used for transport within the arterial wall. The Staverman filtration coefficient in the concentration equation represents the selective permeation of species by the membrane [5,19,23–25].

$$\begin{aligned} &\nabla\cdot\langle\mathbf{V}\rangle=0\\ &\frac{\rho}{\delta}\langle(\mathbf{V}\cdot\nabla)\mathbf{V}\rangle+\frac{\mu}{K}\langle\mathbf{V}\rangle=-\nabla\langle p\rangle+\frac{\mu}{\delta}\nabla^2\langle\mathbf{V}\rangle-\frac{\rho F\delta}{\sqrt{K}}[\langle\mathbf{V}\rangle\cdot\langle\mathbf{V}\rangle]I\\ &\frac{\partial\langle c\rangle}{\partial t}+(1-\sigma_f)\langle\mathbf{V}\rangle\cdot\nabla\langle c\rangle=D_e\nabla^2\langle c\rangle+k\langle c\rangle \end{aligned} \tag{2}$$

where δ is the porosity; K permeability; σ_f the Stavernan filtration coefficient; D_e effective LDL diffusivity, F dimensionless inertia coefficient, I the unit vector oriented along the velocity vector $\mathbf{V}$, k reaction coefficient which is non-zero only inside the media layer and is zero for the other layers. The convective term $\langle(V\cdot\nabla)V\rangle$ is relatively small [24], therefore the momentum equation can be written as

$$-\frac{\mu}{K}\langle V\rangle-\nabla\langle p\rangle+\frac{\mu}{\delta}\nabla^2\langle V\rangle-\frac{\rho F\delta}{\sqrt{K}}[\langle V\rangle\cdot\langle V\rangle]I=0 \tag{3}$$

2.3. Boundary conditions

At the inlet, the lumen is governed by a fully developed parabolic velocity profile

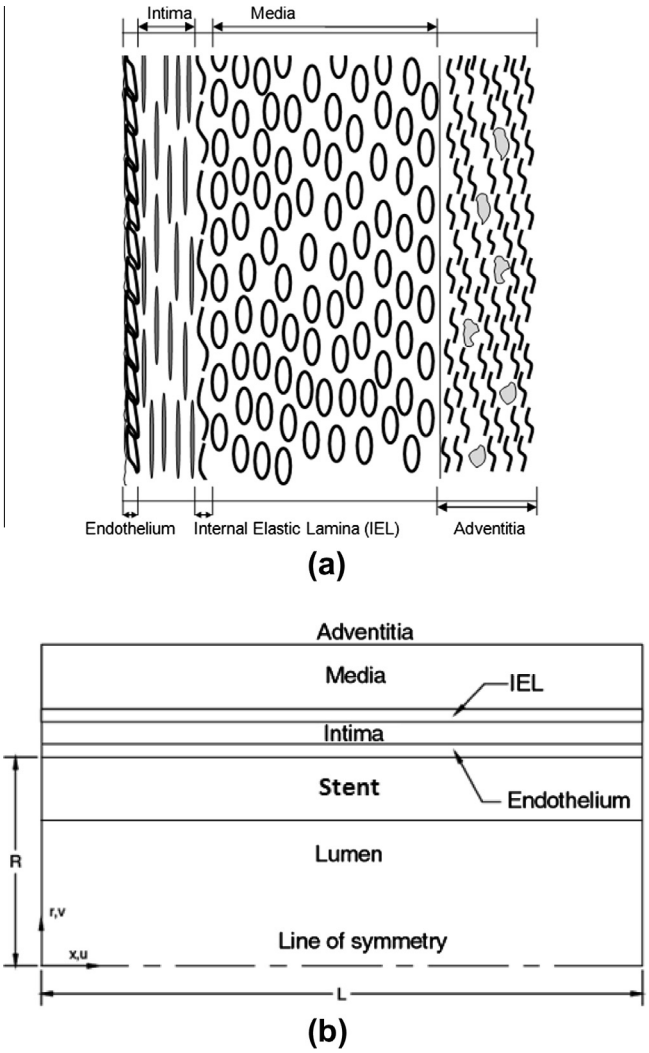

Fig. 1. Schematic of different arterial layers (a) physical display (b) simplified presentation along with the coordinate system.

$$u = u_{\max}(1 - (y/R)^2) \tag{4}$$

where $u_{\max}$ is the centerline velocity, R the radius of the lumen, u the streamwise component of the velocity vector and y is the radial location. According to Yang and Vafai [5]'s research, the impact of pulsation on the LDL transport across the arterial tissue is negligible for a simple straight axisymmetric geometry. Thus it is reasonable here to just consider the steady flow condition.

The velocity at the inlet and outlet within the arterial wall is negligible. The velocity continuity at the interface between different layers is employed and constant pressure at the outlet of the lumen is applied. The boundary conditions on the concentration equations are:

(1) $c/c_0 = 1$ at the lumen inlet and the LDL concentration at the entrance is taken as $c_0 = 28.6 \times 10^{-3}$ mol/m^3[19].
(2) No normal diffusive mass flux at the symmetry axis, lumen outlet and inlet and outlet of the arterial wall.
(3) The species concentration or its derivative is taken to be zero at the media/ adventitia interface.

The continuity of species concentration and the total species flux are incorporated at each interface between the lumen, endothelium, intima, IEL and media. In our analysis, we utilize two adjacent boundaries for each layer and the coordinate system is placed at the interface of the two layers. As such several coordinate systems are utilized in the analysis.

2.4. Physiological properties

The main source of the filtration data is based on the experimental work of Meyer et al. [26]. For a transmural pressure differential of 70 mmHg, the filtration velocity is reported to be $u_{filt} = 1.78 \times 10^{-6}$ cm/s. The total filtration resistance can be expressed as [25]:

$$R_{tot} = \frac{p_1 - p_2}{u_{filt}} = \frac{\mu_{end}L_{end}}{K_{D_{eff,end}}} + \frac{\mu_{int}L_{int}}{K_{D_{eff,int}}} + \frac{\mu_{iel}L_{iel}}{K_{D_{eff,iel}}} + \frac{\mu_{med}L_{med}}{K_{D_{eff,med}}} \tag{5}$$

The Darcy permeability of the intima is hundred fold greater than that in the media and the resistance in the endothelium layer is about a hundred times greater than the one in IEL. The permeability in each layer can be calculated utilizing the experimental data for endothelium, intima, IEL and media, respectively. Table 1 shows the properties in each of the four layers.

The lattice structure of the stent is modeled as a porous medium, thus its morphological properties, such as permeability and effective diffusivity, are required. Assuming a uniform thickness of the metallic struts, the ratio of surface area (opening part to the total part) in the stent would be considered to be the porosity of the stent, as given by

$$\delta_s = \frac{V_{vacant}}{V_{total}} = \frac{A_{opening}}{A_{total}} = 1 - \frac{A_{strut}}{A_{total}} \tag{6}$$

where A_{strut} is the surface area of the metallic struts and A_{total} is the total area of the stent layer.

Permeability of the stent is obtained by Karman–Kozney equation, given by

Table 1
Property values for different arterial layers.

		Lumen	Endothelium	Intima	IEL	Media	Adventitia
Density	ρ [kg/m^3]	1070	1057	1057	1057	1057	1057
Diffusivity	D_{eff} [m^2/s]	2.87E−11	5.706E−18	5.4E−12	3.18E−15	5E−14	
Permeability	K [m^2]		3.22E−21	2E−16	4.392E−19	2E−18	
Porosity	δ		5E−4	0.983	0.002	0.258	
Reaction coefficient	k [s^{-1}]	0	0	0	0	3.197E−4	
Reflection coefficient	σ		0.9888	0.8272	0.9827	0.8836	
Thickness	H^* [μm]	3100	2	10	2	200	100
Viscosity	μ_{eff} [kg/(m s)]	3.7E−3	0.72E−3	0.72E−3	0.72E−3	0.72E−3	
Reynold Number	Re	598.7					
Darcy number	Da		8.05E−10	2.0E−6	1.10E−7	5.00E−11	
Schmidt number	Sc		1.19E+11	1.26E+5	2.14E+8	1.36E+7	

$$K = \frac{d^2}{180}\frac{\delta^3}{(1-\delta)^2} \tag{7}$$

where d is the characteristic length of the stent which is considered to be the width of the stent segment.

The effective mass diffusion coefficient of the stent is represented by

$$D_s = \delta D \tag{8}$$

where δ is the porosity of the stent.

3. Methodology and validation

3.1. Fluid flow analysis

In the lumen and the endothelium layer, the velocity is non-dimensionalized by using a reference velocity given by

$$u_{ch,0} = -\frac{R^2}{2\mu_f}\frac{dp}{dx} \tag{9}$$

The non-dimensional streamwise velocity in the lumen is found to be

$$u_0 = -\eta_{m,0}^2 + 2\eta_{m,0} + U_{0,1} \tag{10}$$

where $\eta_{m,0} = y_0/R$ is the non-dimensional normal coordinate for the lumen and $U_{0,1}$ is the non-dimensional streamwise velocity at the lumen and endothelium interface.

The momentum equation within the endothelium layer becomes

$$\frac{d^2u_1}{d\eta_{m,1}^2} - u_1 - \alpha_1 u_1^2 + 2\delta_1\varepsilon_{m,1}^2 = 0 \tag{11}$$

where $\eta_{m,1} = y_1/\sqrt{K_1/\delta_1}$ is the non-dimensional normal coordinate for the endothelium layer and

$$\alpha_1 = F_1\delta_1 \mathrm{Re}_{ch,1} \tag{12}$$

where $\mathrm{Re}_{ch,1} = (u_{ch,0}\sqrt{K_1})/v_f$ and $u_1 = \langle u_1\rangle/u_{ch,0}$

Expanding u_1 in terms of the powers of the gauge parameter results

$$\begin{aligned} u_1 &= \varepsilon_{m,1}u_{1,1} + \varepsilon_{m,1}^2 u_{1,2} + \varepsilon_{m,1}^3 u_{1,3} \\ \varepsilon_{m,1} &= \frac{1}{R}\sqrt{\frac{K_1}{\delta_1}} \end{aligned} \tag{13}$$

Khakpour and Vafai [19] derived the perturbation solution of the velocity at the interface of lumen and endothelium as

$$U_{0,1} = 2\varepsilon_{m,1} + \left(2\delta_1 - \frac{4\alpha_1}{3}\right)\varepsilon_{m,1}^2 + \left(\frac{20\alpha_1^2}{9} - 4\alpha_1\delta_1\right)\varepsilon_{m,1}^3 \tag{14}$$

For intima, IEL and media layers, the non-dimensional momentum equation becomes

$$\frac{d^2u_i}{d\eta_{m,i}^2} - u_i - \alpha_i u_i^2 + 1 = 0 \tag{15}$$

where the reference velocity is

$$u_{c,i} = -\frac{K_i}{\mu_f}\left(\frac{d\langle p\rangle}{dx}\right) \tag{16}$$

Expanding u_i in terms of powers of porosity, δ_i, results

$$u_i = u_{i,0} + \delta_i u_{i,1} + \delta_i^2 u_{i,2} \tag{17}$$

The perturbation solutions of the velocity at the interfaces of intima and IEL and IEL and Media are obtained as [19]

$$\begin{aligned} U_{0,i} &= U_{i,0} + \delta_i U_{i,1} + \delta_i^2 U_{i,2} \\ U_{i,0} &= \frac{1+\phi_1}{\phi} \\ U_{i,1} &= -\frac{\omega_i}{3\phi}[(U_{i,0})^2\phi_2 + U_{i,0}\phi_3 + \phi_4] \\ U_{i,2} &= \frac{1}{3\phi}\left[\begin{array}{l} -\omega_i U_{i,0}(\phi_3 + 2\phi_2 U_{i,0}) + \\ \omega_i^2(\phi_5(U_{i,0})^3 + \phi_6(U_{i,0})^2 + \phi_7(U_{i,0}) + \phi_8) \end{array}\right]\omega_i = F\mathrm{Re}_i \end{aligned} \tag{18}$$

where

$$\begin{aligned} r_1 &= \frac{K_{i-1}}{K_i}, \quad r_2 = \frac{\delta_{i-1}}{\delta_i} \\ r_3 &= 1, \quad r_4 = \frac{F_{i-1}}{F_i} \end{aligned} \tag{19}$$

$$\begin{aligned} \phi &= 1 + (r_1/r_2)^{1/2} \\ \phi_1 &= (r_1/r_2)^{1/2}(r_1 r_3)^{-1} \\ \phi_2 &= 1 + (r_4 r_2^{3/2})^{-1} \\ \phi_3 &= 1 + (r_1 r_4 r_3 r_2^{3/2})^{-1} \\ \phi_4 &= 1 + (r_1^2 r_4 r_3^2 r_2^{3/2})^{-1} \\ \phi_5 &= 1 + (r_1^{1/2} r_4^2 r_2^{5/2})^{-1} \\ \phi_6 &= 1 + (r_1^{3/2} r_4^2 r_3 r_2^{5/2})^{-1} \\ \phi_7 &= 1 + (r_1^{5/2} r_4^2 r_3^2 r_2^{5/2})^{-1} \\ \phi_8 &= 1 + (r_1^{7/2} r_4^2 r_3^3 r_2^{5/2})^{-1} \end{aligned} \tag{20}$$

The filtration velocity in the direction normal to the luminal blood flow is calculated by Darcy's law given by

$$\mathrm{v} = -\frac{K_{wall}}{\mu_f}\frac{\Delta p}{l}\Big|_{wall} \tag{21}$$

where $\frac{\Delta p}{l}|_{wall}$ is the transmural pressure gradient and K_{wall} is the average permeability of the arterial wall.

3.2. Mass transport

3.2.1. Mass transport without a reaction

The governing species conservation equation without a reaction term is given by

$$(1-\sigma_f)\left(\langle u\rangle\frac{\partial\langle c\rangle}{\partial x} + \langle \mathrm{v}\rangle\frac{\partial\langle c\rangle}{\partial y}\right) = D\frac{\partial^2\langle c\rangle}{\partial y^2} \tag{22}$$

The non-dimensional form of the species equation can be written as

$$\left(\frac{\mathrm{v}L}{\sqrt{\frac{K_i/\delta_i}{Sc_i}}}\right)\frac{\partial N_i}{\partial\eta_{s,i}} + u_i\frac{\partial N_i}{\partial\xi} = \frac{1}{\mathrm{Re}_i\sqrt{Da_i}}\frac{\partial^2 N_i}{\partial\eta_{s,i}^2} \tag{23}$$

where

$$\begin{aligned} &\xi = \tfrac{x}{L}, \quad u = \tfrac{1-\sigma_f}{\delta}\tfrac{\langle u\rangle}{u_{ch}}, \quad \mathrm{v} = \tfrac{1-\sigma_f}{\delta}\tfrac{\langle \mathrm{v}\rangle}{u_{ch}}, \\ &\eta_s = y\sqrt{\tfrac{Sc}{K/\delta}}, \quad N = \tfrac{c}{C_{ref}} \end{aligned}$$

The non-dimensionalization of spatial variable y is different from the one used in velocity Eqs. (10), (11) and (15).

Utilizing $V_i = \frac{vL}{\sqrt{\frac{K_i/\delta}{Sc_i}}}$ and $u_i = U_{0,i} + \Lambda_i\eta_{s,i}Sc_i^{-1/2}$ results the following form for Eq. (23)

$$V_i\frac{\partial N_i}{\partial\eta_{s,i}} + (U_{0,i} + \Lambda_i\eta_{s,i}Sc_i^{-1/2})\frac{\partial N_i}{\partial\xi} = \frac{1}{\mathrm{Re}_i\sqrt{Da_i}}\frac{\partial^2 N_i}{\partial\eta_{s,i}^2} \tag{24}$$

where

$$\Lambda_0 = \frac{2}{R}\sqrt{k_1}$$

$$\Lambda_1 = -\frac{1}{R}\sqrt{\frac{k_1}{\delta_1}}$$

$$\Lambda_i = (1-U_{0,i}^0) - \delta_i\left[U_{0,i}^1 + \frac{\beta_1}{3}\left(\left(U_{0,i}^0\right)^2 + U_{0,i}^0 + 1\right)\right] - \delta_i^2\left[\begin{array}{l} U_{0,i}^2 + \frac{\beta_1 U_{0,i}^1}{3}(2U_{0,i}^0+1) + \\ \frac{\beta_1^2 U_{0,i}^1}{18}\left(7\left(U_{0,i}^0\right)^3 - 11\left(U_{0,i}^0\right)^2 - 62U_{0,i}^0 + 72\right)\end{array}\right]$$

and $i = 0, 1, 2, 3, 4$ designates lumen, endothelium, intima, IEL and media respectively.

In order to solve Eq. (24), the concentration field is expanded in terms of $Sc^{-1/2}$ as

$$N_i = N_i^0 + Sc_i^{-1/2} N_i^1 \tag{25}$$

The expansion of the species concentration field results in the zeroth- and first-order equations as

$$\begin{aligned} V_i\frac{\partial N_i^0}{\partial \eta_{s,i}} + U_{0,i}\frac{\partial N_i^0}{\partial \xi} &= \frac{1}{\mathrm{Re}_i\sqrt{Da_i}}\frac{\partial^2 N_i^0}{\partial \eta_{s,i}^2} \\ V_i\frac{\partial N_i^1}{\partial \eta_{s,i}} + U_{0,i}\frac{\partial N_i^1}{\partial \xi} + \Lambda_i\eta_{s,i}\frac{\partial N_i^0}{\partial \xi} &= \frac{1}{\mathrm{Re}_i\sqrt{Da_i}}\frac{\partial^2 N_i^1}{\partial \eta_{s,i}^2} \end{aligned} \tag{26}$$

The inlet and interface conditions are given by

$$\begin{aligned} N_i(\xi=0,\eta_{s,i}) &= 0 \\ N_i(\xi,\eta_{s,i}=0) &= f_i(\xi) \end{aligned} \tag{27}$$

where $f_i(\xi)$ is the non-dimensional concentration at the interface.

Defining the Laplace transformation in the ξ domain of N_i^0:

$$L\left(N_i^0\right) = Z(s,\eta_{s,i})$$

$$L\left(\frac{\partial N_i^0}{\partial \xi}\right) = sZ(s,\eta_{s,i})$$

Defining the Laplace transformation in the ξ domain of N_i^1:

$$L\left(N_i^1\right) = Y(s,\eta_{s,i})$$

$$L\left(\frac{\partial N_i^1}{\partial \xi}\right) = sY(s,\eta_{s,i})$$

Applying the Laplace transformation in the ξ domain to Eq. (26):

$$\begin{aligned} V_i\frac{\partial Z}{\partial \eta_{s,i}} + U_{0,i}sZ &= \frac{1}{\mathrm{Re}_i\sqrt{Da_i}}\frac{\partial^2 Z}{\partial \eta_{s,i}^2} \\ V_i\frac{\partial Y}{\partial \eta_{s,i}} + U_{0,i}sY + \Lambda_i\eta_{s,i}sZ &= \frac{1}{\mathrm{Re}_i\sqrt{Da_i}}\frac{\partial^2 Y}{\partial \eta_{s,i}^2} \end{aligned} \tag{28}$$

Using the Laplace transformation, the zeroth- and first-order solution of Eq. (28) for layer i and $i+1$ are found to be

$$zeroth: Z_i = \frac{1}{1+\frac{c_{i+1}}{c_i}\sqrt{\frac{c_{i+1}}{c_i}}\sqrt{\frac{r_2 r_5}{r_1}}}\left(\frac{1}{s-J} - \frac{4c_{i+1}}{s^2-Js}\right) \times \exp\left(\frac{A_i - \sqrt{A_i^2+4B_i s}}{2}\eta_{s,i}\right)$$

$$first: Y_i = h_i\exp\left(\frac{A_i - \sqrt{A_i^2+4B_i s}}{2}\eta_{s,i}\right) + \left[\begin{array}{l} -\frac{\Lambda_i \mathrm{Re}_i\sqrt{Da_i}}{\sqrt{A_i^2+4B_i s}}n_i\eta_{s,i}\left(\frac{1}{2}\eta_{s,i} + \frac{1}{\sqrt{A_i^2+4B_i s}}\right) \\ \exp\left(\frac{A_i-\sqrt{A_i^2+4B_i s}}{2}\eta_{s,i}\right)\end{array}\right]$$

$$zeroth: Z_{i+1} = \left[\frac{1}{s} - \frac{1}{1+\frac{c_{i+1}}{c_i}\sqrt{\frac{c_{i+1}}{c_i}}\sqrt{\frac{r_2 r_5}{r_1}}}\left(\frac{1}{s-J} - \frac{4c_{i+1}}{s^2-Js}\right)\right] \times \exp\left(\frac{A_{i+1} - \sqrt{A_{i+1}^2+4B_{i+1}s}}{2}\eta_{s,i+1}\right)$$

$$first: Y_{i+1} = -r_5^{1/2}h_i\exp\left(\frac{A_{i+1} - \sqrt{A_{i+1}^2+4B_{i+1}s}}{2}\eta_{s,i+1}\right) + \left[\begin{array}{l} -\frac{\Lambda_{i+1}\mathrm{Re}_{i+1}\sqrt{Da_{i+1}}}{\sqrt{A_{i+1}^2+4B_{i+1}s}}n_{i+1}\eta_{s,i+1} \\ \left(\frac{1}{2}\eta_{s,i+1} + \frac{1}{\sqrt{A_{i+1}^2+4B_{i+1}s}}\right)\exp\left(\frac{A_{i+1}-\sqrt{A_{i+1}^2+4B_{i+1}s}}{2}\eta_{s,i+1}\right)\end{array}\right] \tag{29}$$

where

$$A_i = V_i\mathrm{Re}_{ch,i}\sqrt{Da_i},\quad B_i = U_{0,i}\mathrm{Re}_{ch,i}\sqrt{Da_i},\quad c_i = \frac{V_i^2(\mathrm{Re}_{ch,i}\sqrt{Da_i})}{4U_{0,i}},$$

$$r_5 = D_i/D_{i+1}$$

$$J = \frac{1+\sqrt{\frac{c_{i+1}}{c_i}}\sqrt{\frac{r_2 r_5}{r_1}}}{\frac{1}{4c_{i+1}}+\frac{1}{4c_i}\sqrt{\frac{c_{i+1}}{c_i}}\sqrt{\frac{r_2 r_5}{r_1}}},\quad n_i = \frac{1}{1+\frac{c_{i+1}}{c_i}\sqrt{\frac{c_{i+1}}{c_i}}\sqrt{\frac{r_2 r_5}{r_1}}}\left(\frac{1}{s-J} - \frac{4c_{i+1}}{s^2-Js}\right),$$

$$n_{i+1} = \frac{1}{s} - n_i$$

$$h_i = \frac{4\left[\left(\sqrt{\frac{r_2 r_5^2}{r_1}}\frac{\Lambda_i\mathrm{Re}_i\sqrt{Da_i}}{B_i(s+c_i)} + \frac{\Lambda_{i+1}\mathrm{Re}_{i+1}\sqrt{Da_{i+1}}}{B_{i+1}(s+c_{i+1})}\right)n_i - \frac{\Lambda_{i+1}\mathrm{Re}_{i+1}\sqrt{Da_{i+1}}}{sB_{i+1}(s+c_{i+1})}\right]}{\sqrt{\frac{r_2 r_5^2}{r_1}}\frac{A_i}{c_i^2}s(s-4c_i) + \sqrt{r_5}\frac{A_{i+1}}{c_{i+1}^2}s(s-4c_{i+1})}$$

Applying the inverse Laplace transformation to Eq. (29), the concentration distributions are found to be

For the *i*th layer:

$$N_i = N_i^0 + Sc_i^{-1/2}N_i^1$$

where

$$N_i^0 = \frac{1}{1+\frac{c_{i+1}}{c_i}\sqrt{\frac{c_{i+1}}{c_i}}\sqrt{\frac{r_2 r_5}{r_1}}}\exp\left(\frac{A_i}{2}\eta_{s,i}\right)\left(1-\frac{4c_{i+1}}{J}\right) \times \left[\left(1-q_{1,i}^{1/2}+\frac{q_{1,i}}{2}\right)+J\left(\frac{q_{2,i}}{2}-\frac{q_{1,i}^{1/2}}{2c_i}\right)+J^2\frac{q_{1,i}^{1/2}}{8c_i^2}\right] \times \exp(J\xi) + \frac{1}{1+\frac{c_{i+1}}{c_i}\sqrt{\frac{c_{i+1}}{c_i}}\sqrt{\frac{r_2 r_5}{r_1}}} \times \exp\left(\frac{A_i}{2}\eta_{s,i}\right)\frac{4c_{i+1}}{J}erfc\left(\frac{B_i^{1/2}\eta_{s,i}}{2\sqrt{\xi}}\right)$$

and $N_i^1 = N_{i,1}^1 + N_{i,2}^1$

$$N_{i,2}^1 = -\frac{\Lambda_i\mathrm{Re}_i\sqrt{Da_i}(1+\exp(J\xi))}{1+\frac{c_{i+1}}{c_i}\sqrt{\frac{c_{i+1}}{c_i}}\sqrt{\frac{r_2 r_5}{r_1}}}\eta_{s,i}\exp\left(\frac{A_i}{2}\eta_{s,i}\right) \left\{\begin{array}{l} \frac{-c_{i+1}\sqrt{B_i}}{2J\sqrt{\pi}\sqrt{\xi}}\exp(-c_i\xi)\eta_{s,i}^3 \\ +\left[\frac{4c_{i+1}}{A_i^2 J}(1-\exp(-c_i\xi)) - \frac{\sqrt{B_i}c_{i+1}}{J}\eta_{s,i}\right] \\ erfc\left(\frac{B_i^{1/2}\eta_{s,i}}{2\sqrt{\xi}}\right)\end{array}\right\}$$

and

$$N_{i,1}^1 = \frac{4}{\sqrt{\frac{r_2 r_5^2}{r_1}\frac{A_i}{c_i^2} + \sqrt{r_5}\frac{A_{i+1}}{c_{i+1}^2}}} \exp\left(\frac{A_i}{2}\eta_{s,i}\right) erfc\left(\frac{B_i^{1/2}\eta_{s,i}}{2\sqrt{\xi}}\right) *$$

$$\left[\begin{array}{l} \frac{1}{1+\frac{c_{i+1}}{c_i}\sqrt{\frac{c_{i+1}}{c_i}}\sqrt{\frac{r_2 r_5}{r_1}}} \\ \left(\begin{array}{l} \sqrt{\frac{r_2 r_5^2}{r_1}}\frac{\Lambda_i \mathrm{Re}_i\sqrt{Da_i}}{B_i}\left(\begin{array}{l} -\frac{\exp(-c_i\xi)}{c_i(c_i+J)(c_i+H)} + \frac{\exp(J\xi)}{J(c_i+J)(J-H)} \\ +\frac{\exp(H\xi)}{H(c_i+H)(H-J)} + \frac{1}{c_i HJ} \end{array}\right) \\ -\sqrt{\frac{r_2 r_5^2}{r_1}}\frac{4c_{i+1}\Lambda_i \mathrm{Re}_i\sqrt{Da_i}}{B_i}\left(\begin{array}{l} \frac{cJ-JH+c_iH}{c_i^2 JH} + \frac{\exp(-c_i\xi)}{c_i^2(c_i+J)(c_i+H)} + \\ \frac{\exp(J\xi)}{J^2(c_i+J)(J-H)} + \frac{\exp(H\xi)}{H^2(c_i+H)(H-J)} \\ +\frac{\xi}{c_i HJ} \end{array}\right) \\ +\frac{\Lambda_{i+1}\mathrm{Re}_{i+1}\sqrt{Da_{i+1}}}{B_{i+1}}\left(\begin{array}{l} -\frac{\exp(-c_{i+1}\xi)}{c_{i+1}(c_{i+1}+J)(c_{i+1}+H)} + \frac{\exp(J\xi)}{J(c_{i+1}+J)(J-H)} \\ +\frac{\exp(H\xi)}{H(c_{i+1}+H)(H-J)} + \frac{1}{c_{i+1}HJ} \end{array}\right) \\ -\frac{4c_{i+1}\Lambda_{i+1}\mathrm{Re}_{i+1}\sqrt{Da_{i+1}}}{B_{i+1}}\left(\begin{array}{l} \frac{c_{i+1}J-JH+c_{i+1}H}{c_{i+1}^2 JH} + \frac{\exp(-c_{i+1}\xi)}{c_{i+1}^2(c_{i+1}+J)(c_{i+1}+H)} + \\ \frac{\exp(J\xi)}{J^2(c_{i+1}+J)(J-H)} + \frac{\exp(H\xi)}{H^2(c_{i+1}+H)(H-J)} \\ +\frac{\xi}{c_{i+1}HJ} \end{array}\right) \end{array}\right) \\ -\frac{\Lambda_{i+1}\mathrm{Re}_{i+1}\sqrt{Da_{i+1}}}{B_{i+1}}\left(\begin{array}{l} \frac{H-c_{i+1}}{c_{i+1}^2 H} - \frac{\exp(-c_{i+1}\xi)}{c_{i+1}^2(c_{i+1}+H)} \\ +\frac{\exp(H\xi)}{H^2(c_{i+1}+H)} - \frac{\xi}{c_{i+1}H} \end{array}\right) \end{array}\right] \tag{30}$$

where

$$H = \frac{\frac{4A_i}{c_i}\sqrt{\frac{r_2 r_5^2}{r_1}} + \frac{4A_{i+1}}{c_{i+1}}\sqrt{r_5}}{\frac{A_i}{c_i^2}\sqrt{\frac{r_2 r_5^2}{r_1}} + \frac{A_{i+1}}{c_{i+1}^2}\sqrt{r_5}}$$

For the $(i+1)$th layer:

$$N_{i+1} = N_{i+1}^0 + Sc_{i+1}^{-1/2} N_{i+1}^1$$

where

$$\begin{aligned} N_{i+1}^0 = &-\frac{1}{1+\frac{c_{i+1}}{c_i}\sqrt{\frac{c_{i+1}}{c_i}}\sqrt{\frac{r_2 r_5}{r_1}}}\left(1-\frac{4c_{i+1}}{J}\right) \\ &\times\left[\left(1-q_{1,i+1}^{1/2}+\frac{q_{1,i+1}}{2}\right)+J\left(\frac{q_{2,i+1}}{2}-\frac{q_{1,i+1}^{1/2}}{2c_{i+1}}\right)+J^2\frac{q_{1,i+1}^{1/2}}{8c_{i+1}^2}\right] \\ &\times\exp\left(\frac{A_{i+1}}{2}\eta_{s,i+1}\right)\exp(J\xi)+\left(1-\frac{1}{1+\frac{c_{i+1}}{c_i}\sqrt{\frac{c_{i+1}}{c_i}}\sqrt{\frac{r_2 r_5}{r_1}}}\frac{4c_{i+1}}{J}\right) \\ &\times\exp\left(\frac{A_{i+1}}{2}\eta_{s,i+1}\right)erfc\left(\frac{B_{i+1}^{1/2}\eta_{s,i+1}}{2\sqrt{\xi}}\right) \end{aligned}$$

and

$$N_{i+1}^1 = N_{i+1,1}^1 + N_{i+1,2}^1$$

where

$$N_{i+1,1}^1 = -r_5^{1/2} N_{i,1}^1$$

and

$$\begin{aligned} N_{i+1,2}^1 = &-\Lambda_{i+1}\mathrm{Re}_{i+1}\sqrt{Da_{i+1}}\exp(-c_1\xi)\eta_{s,i+1}\exp\left(\frac{A_{i+1}}{2}\eta_{s,i+1}\right) \\ &\times\left[\left(1-\frac{B_{i+1}}{2}\eta_{s,i+1}\right)erfc\left(\frac{B_{i+1}^{1/2}\eta_{s,i+1}}{2\sqrt{\xi}}\right)-\frac{B_{i+1}}{4\sqrt{\pi}\sqrt{\xi}}\eta_{s,i+1}^3\right] \\ &+\frac{\Lambda_{i+1}\mathrm{Re}_{i+1}\sqrt{Da_{i+1}}(1+\exp(J\xi))}{1+\frac{c_{i+1}}{c_i}\sqrt{\frac{c_{i+1}}{c_i}}\sqrt{\frac{r_2 r_5}{r_1}}} \\ &\eta_{s,i+1}\exp\left(\frac{A_{i+1}}{2}\eta_{s,i+1}\right)\left\{\begin{array}{l} \frac{-c_{i+1}\sqrt{B_{i+1}}}{2J\sqrt{\pi}\sqrt{\xi}}\exp(-c_{i+1}\xi)\eta_{s,i+1}^3 \\ +\left[\frac{4c_{i+1}}{A_{i+1}^2 J}(1-\exp(-c_{i+1}\xi))-\frac{\sqrt{B_{i+1}}c_{i+1}}{J}\eta_{s,i+1}\right] \\ erfc\left(\frac{B_{i+1}^{1/2}\eta_{s,i+1}}{2\sqrt{\xi}}\right) \end{array}\right\} \end{aligned} \tag{31}$$

where

$$q_{1,i} = \frac{A_i^2\eta_{s,i}^2}{4}$$
$$q_{2,i} = B_i\eta_{s,i}^2$$

Eqs. (30) and (31) can be applied to find the species concentration profile within endothelium, intima and IEL.

3.2.2. Mass transport in the presence of a reaction

The chemical reaction should be considered for the mass transport within the media layer, which is modeled as an irreversible first-order reaction. The species concentration equation for the media layer can be written as

$$(1-\sigma_f)\langle V\rangle\cdot\nabla\langle c\rangle = D\nabla^2\langle c\rangle + k\langle c\rangle \tag{32}$$

where k is the chemical reaction rate.

The non-dimensional form of the species concentration equation within the media layer is given by

$$V\frac{\partial N_4}{\partial\eta_{s,4}} + (U_{0,4}+\Lambda_4\eta_{s,4}Sc_4^{-1/2})\frac{\partial N_4}{\partial\xi} = \frac{1}{\mathrm{Re}_4\sqrt{Da_4}}\frac{\partial^2 N_4}{\partial\eta_{s,4}^2} - r_c N_4 \tag{33}$$

where

$$r_c = -\frac{kL}{u_{ch,4}\delta_4}$$

In order to solve Eq. (33), the concentration field is expanded in terms of $Sc^{-1/2}$ as

$$N_4 = N_4^0 + Sc_4^{-1/2}N_4^1 \tag{34}$$

The expansion of the species concentration field results in the zeroth- and first-order equations as

$$\begin{aligned} &V\frac{\partial N_4^0}{\partial\eta_{s,4}} + U_{0,4}\frac{\partial N_4^0}{\partial\xi} = \frac{1}{\mathrm{Re}_4\sqrt{Da_4}}\frac{\partial^2 N_4^0}{\partial\eta_{s,4}^2} - r_c N_4^0 \\ &V\frac{\partial N_4^1}{\partial\eta_{s,4}} + U_{0,4}\frac{\partial N_4^1}{\partial\xi} + \Lambda_4\eta_{s,4}\frac{\partial N_4^0}{\partial\xi} = \frac{1}{\mathrm{Re}_4\sqrt{Da_4}}\frac{\partial^2 N_4^1}{\partial\eta_{s,4}^2} - r_c N_4^1 \end{aligned} \tag{35}$$

Using the same Laplace transform in the ξ domain in Eqs. (28)–(35):

$$\begin{aligned} &V\frac{\partial Z}{\partial\eta_{s,4}} + U_{0,4}sZ = \frac{1}{\mathrm{Re}_4\sqrt{Da_4}}\frac{\partial^2 Z}{\partial\eta_{s,4}^2} - r_c Z \\ &V\frac{\partial Y}{\partial\eta_{s,4}} + U_{0,4}sY + \Lambda_4\eta_{s,4}sZ = \frac{1}{\mathrm{Re}_4\sqrt{Da_4}}\frac{\partial^2 Y}{\partial\eta_{s,4}^2} - r_c Y \end{aligned} \tag{36}$$

The Laplace solution for the above species concentration equations within the media layer is obtained as

$$zeroth: Z_4 = \left[\frac{1}{s} - \frac{1}{1+\frac{c_4}{c_3}\sqrt{\frac{c_4}{c_3}}\sqrt{\frac{r_2 r_5}{r_1}}}\left(\frac{1}{s-J} - \frac{4c_4}{s^2 - Js}\right)\right] \times \exp\left(\frac{A_4 - \sqrt{A_4^2 + 4B_4 s + 4\gamma}}{2}\eta_{s,4}\right)$$

$$first: Y_4 = -r_5^{1/2} h_3 \exp\left(\frac{A_4 - \sqrt{A_4^2 + 4B_4 s + 4\gamma}}{2}\eta_{s,4}\right) + \left[-\frac{\Lambda_4 \mathrm{Re}_4 \sqrt{Da_4}}{\sqrt{A_4^2 + 4B_4 s + 4\gamma}} n_4 \eta_{s,4} \times \left(\frac{1}{2}\eta_{s,4} + \frac{1}{\sqrt{A_4^2 + 4B_4 s + 4\gamma}}\right) \times \exp\left(\frac{A_4 - \sqrt{A_4^2 + 4B_4 s + 4\gamma}}{2}\eta_{s,4}\right)\right] \quad (37)$$

where subscript 3 refers to parameters in IEL, and subscript 4 refers to parameters in media and $\gamma = r_c \mathrm{Re}_4 \sqrt{Da_4}$.

The concentration distribution in the media layer is found to be

$$N_4 = N_4^0 + Sc_4^{-1/2} N_4^1 \quad (38)$$

where

$$N_4^0 = -\frac{1}{1+\frac{c_4}{c_3}\sqrt{\frac{c_4}{c_3}}\sqrt{\frac{r_2 r_5}{r_1}}}\left[\left(\frac{A_4^2}{8} + \frac{B_4 J}{2}\right)\eta_4^2 - \left(\frac{A_4}{2} + \frac{A_4 J}{4(c_4+\beta_4)} - \frac{J^2 A_4^2}{16(c_4+\beta_4)^{1/2}}\right)\eta_4 + 1\right]\left(1 - \frac{4c_4}{J}\right) \times \exp\left(\frac{A_4}{2}\eta_{s,4}\right)\exp(J\xi) + \left(1 - \frac{1}{1+\frac{c_4}{c_3}\sqrt{\frac{c_4}{c_3}}\sqrt{\frac{r_2 r_5}{r_1}}}\frac{4c_4}{J}\right) \times \exp\left(\frac{A_4}{2}\eta_{s,4}\right) erfc\left(\frac{B_4^{1/2}\eta_{s,4}}{2\sqrt{\xi}}\right)$$

and

$$N_4^1 = N_{4,1}^1 + N_{4,2}^1$$

where

$$N_{4,1}^1 = -r_5^{1/2} N_{3,1}^1$$

and

$$N_{4,2}^1 = -\Lambda_4 \mathrm{Re}_4 \sqrt{Da_4}\exp(-(c_4+\beta_4)\xi)\eta_{s,4}\exp\left(\frac{A_4}{2}\eta_{s,4}\right)\left[\left(1 - \frac{B_4}{2}\eta_{s,4}\right) erfc\left(\frac{B_4^{1/2}\eta_{s,4}}{2\sqrt{\xi}}\right) - \frac{B_4}{4\sqrt{\pi}\sqrt{\xi}}\eta_{s,4}^3\right] + \frac{\Lambda_4 \mathrm{Re}_4 \sqrt{Da_4}(1+\exp(J\xi))}{1+\frac{c_4}{c_3}\sqrt{\frac{c_4}{c_3}}\sqrt{\frac{r_2 r_5}{r_1}}} \eta_{s,4}\exp\left(\frac{A_4}{2}\eta_{s,4}\right)\left\{\begin{array}{l} \frac{-c_4\sqrt{B_4}}{2J\sqrt{\pi}\sqrt{\xi}}\exp(-(c_4+\beta_4)\xi)\eta_{s,4}^3 + \\ \left[\frac{4c_4}{A_4^2 J}(1-\exp(-(c_4+\beta_4)\xi)) - \frac{\sqrt{B_4}c_4}{J}\eta_{s,4}\right] \\ erfc\left(\frac{B_4^{1/2}\eta_{s,4}}{2\sqrt{\xi}}\right) \end{array}\right\}$$

where $\beta_4 = k/U_{0,4}$

It should be noted that Eqs. (29)–(38) incorporate corrections over the results presented in Khakpour and Vafai [19].

4. Results and discussion

Property values for different layers are given in Table 1. The average arterial permeability is found to be $K_{wall} = 3.77 \times 10^{-19}\ \mathrm{m}^2$. The filtration velocities are respectively calculated to be 2.283×10^{-8} m/s and 5.218×10^{-8} m/s for transmural pressure differentials of 70 mmHg and 160 mmHg respectively, which is also reported by Khakpour and Vafai [19].

Using Eqs. (18)–(20), the streamwise velocity at each interface can be obtained. The results are presented in Table 2. Both the

Table 2
Streamwise velocity at the interface of different arterial layers.

Interface streamwise velocity	m/s	Interface
$U_{0,1}$	2.6921E−06	Lumen/endothelium
$U_{0,2}$	1.9513E−08	Endothelium/intima
$U_{0,3}$	1.36458E−13	Intima/IEL
$U_{0,4}$	5.5638E−14	IEL/media

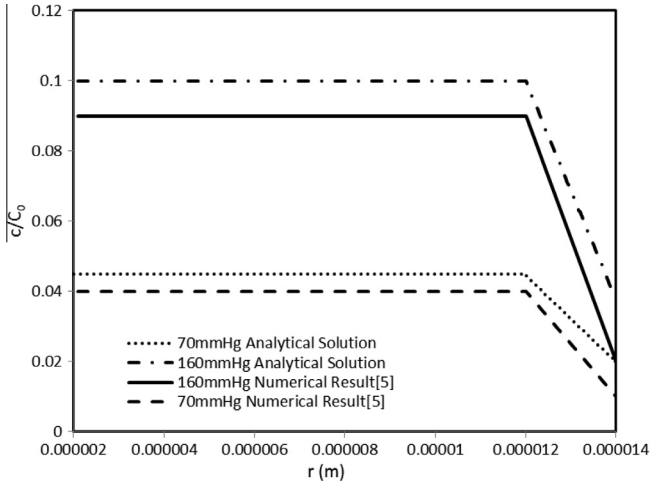

Fig. 2. Radial variation of normalized LDL concentration across intima and IEL layers-comparison between analytical and numerical results ($x = 60$ mm, $L = 124$ mm).

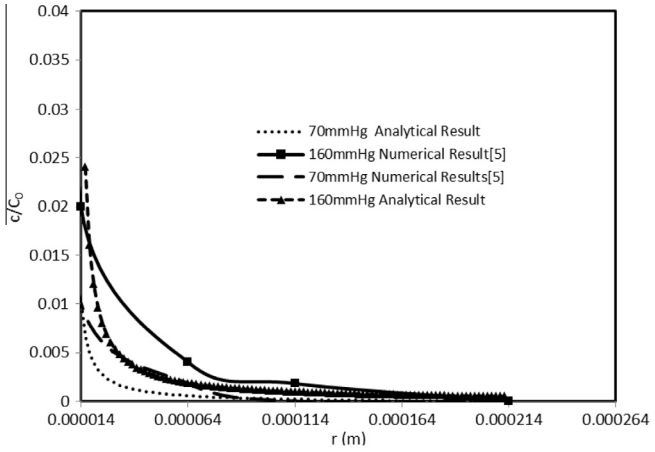

Fig. 3. Radial variation of normalized LDL concentration across the media layer-comparison between analytical and numerical results ($x = 60$ mm).

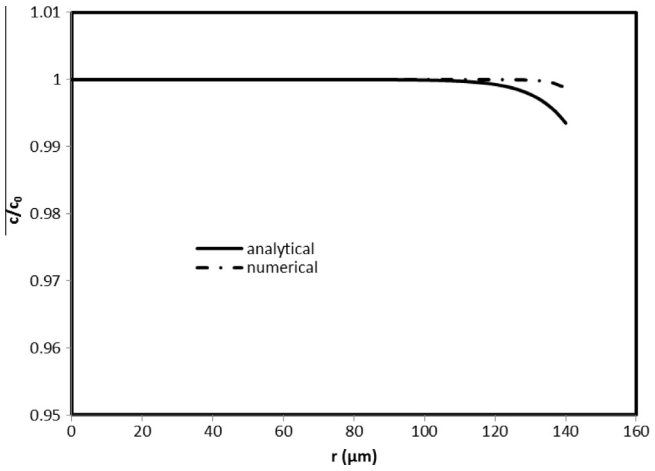

Fig. 4. Numerical and analytical LDL concentration distribution in radial direction across the stent.

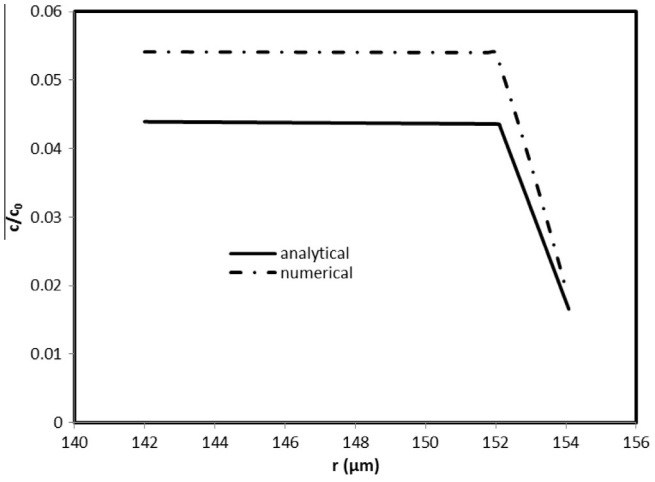

Fig. 5. Numerical and analytical LDL concentration distributions across the intima and IEL layers in the presence of a stent.

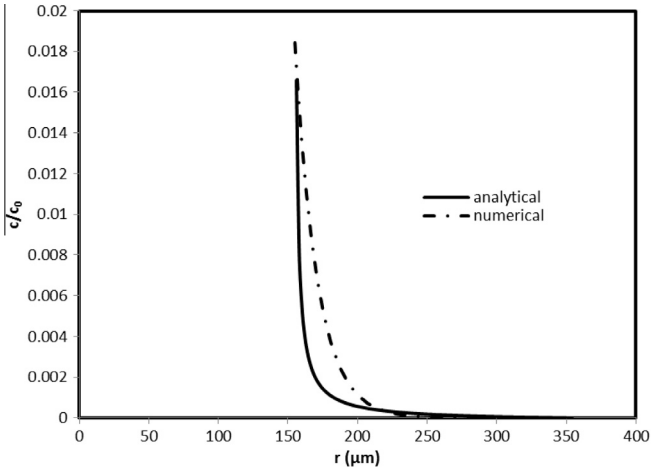

Fig. 6. Numerical and analytical LDL concentration distributions across the media layer.

filtration and the streamwise velocities at each interface are needed to obtain the species concentration distribution.

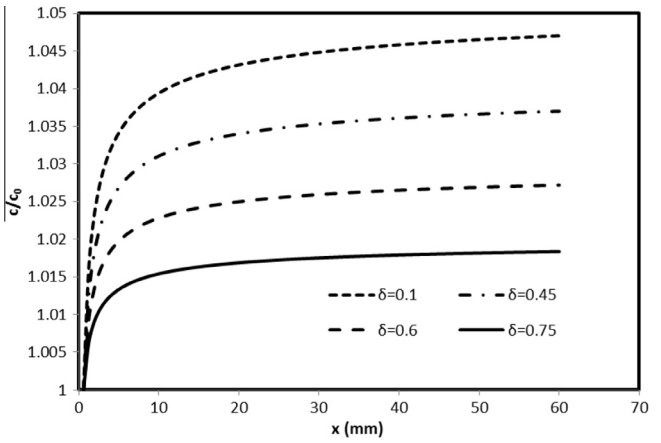

Fig. 7. Axial variation of analytical normalized LDL concentration at the interface of lumen and the stent-Effect of the stent compactness represented through porosity variation.

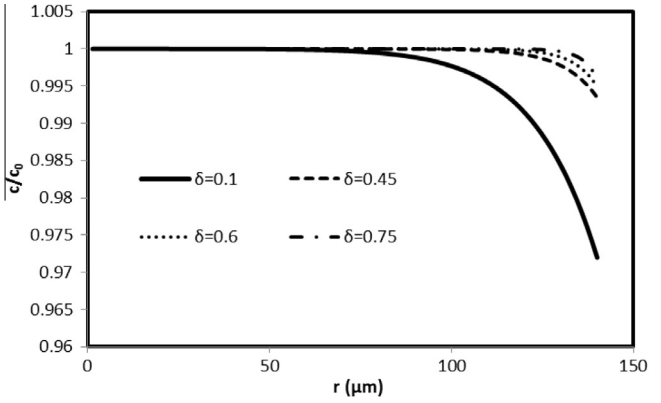

Fig. 8. Analytical LDL concentration distributions in the radial direction in stents with different porosities–Effect of variations in the stent compactness, represented through porosity variation, on the LDL concentration distribution across the stent.

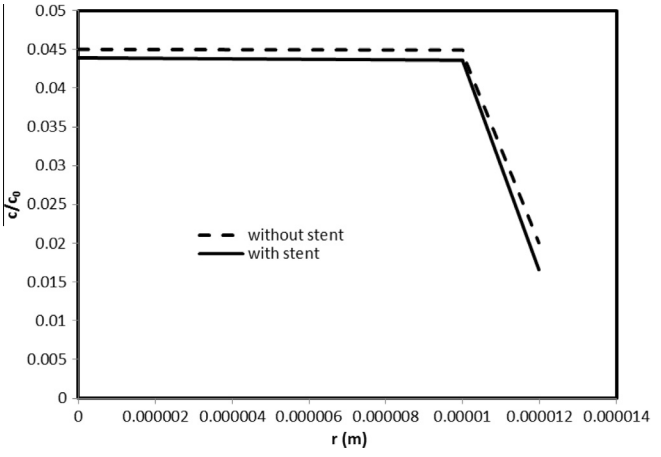

Fig. 9. Analytical LDL concentration distribution in radial direction across the Intima and IEL with and without the stent.

The radial variation of LDL concentration across intima and IEL layers under transmural pressure differentials of 160 mmHg and 70 mmHg is presented in Fig. 2. The corresponding LDL concentra-

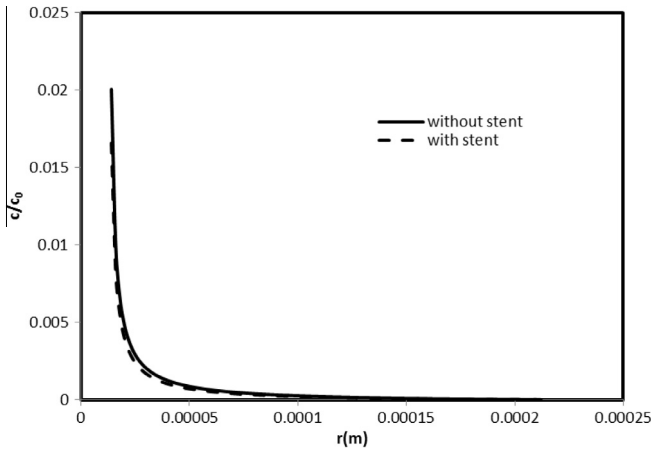

Fig. 10. Analytical LDL concentration distribution in the radial direction across the media with and without the stent.

tion distributions within the media layer under different transmural pressure differentials are shown in Fig. 3. The governing species conservation equation in Fig. 2 is different from the one in Fig. 3. There is a reaction term for the mass transport in the media layer in Fig. 3. The analytical approximation for the reaction term would make the result larger than the numerical solution. It should be noted that this result does not conflict with the result shown in Fig. 2. The results are in good agreement with the numerical solution of Yang and Vafai [5]. Due to the reaction term, the concentration distributions within the media layer are nonlinear while in intima and IEL layers, the radial variations of concentration are nearly linear. With an increase in the transmural pressure differential, the value of normalized concentration in each arterial layer increases. Thus hypertension would aggravate the species accumulation within the arterial wall.

The stent is modeled as a porous medium. The size and morphological properties of the stent in the numerical model are in par with the analytical model. The numerical and analytical concentration distributions in stent, intima, IEL and media are presented in Figs. 4–6 and are found to be in good agreement. The numerical results yield values which are larger than the analytical results.

4.1. Effect of stent on the LDL concentration distribution

The lattice structure of the stent is modeled as a porous medium in the analytical model. The analytical solutions given earlier are modified to incorporate the stent layer. Stents morphological properties, such as permeability and effective diffusivity, are obtained from Eqs. (6)–(8). In the analytical model, the compactness of the stent is analyzed through use of a range of porosities given by $0.1, 0.45, 0.6, 0.75$ [27,28]. The corresponding permeabilities are calculated to be $4.535 \times 10^{-13}, 6.69 \times 10^{-11}, 3 \times 10^{-10}, 1.5 \times 10^{-9}$ m^2. The diffusivity for a porosity of $\delta_s = 0.1$ is 10^{-14} m^2/s [27,28]. The transmural pressure differential is taken to be 70 mmHg and the thickness of the stent is taken as 140 μm [29].

Fig. 7 shows the axial concentration distribution at the interface of lumen and the stent. As can be seen as the stent becomes more compact, LDL accumulation at the interface increases. The effect of variations in the stent compactness, represented through the porosity variation on the radial concentration distribution, is shown in Fig. 8. It can be seen that the concentration at the interface between the stent and the endothelium decreases as the stent compactness increases.

Figs. 9 and 10 display the effect of the stent on the concentration distributions in intima, IEL and media respectively. As can be seen in Figs. 9 and 10, the stent has a minimal effect on the concentration distribution in these layers.

5. Conclusions

A detailed and comprehensive analytical solution of the macromolecular transport within an arterial wall is presented in this work. The solution is obtained through the application of singular perturbation analysis along with Laplace and inverse Laplace transformations. Detailed analytical results are obtained for the velocity and species concentration distributions within different arterial layers. The analytical results are found to be in good agreement with the numerical results.

The stent with the latticed structure is modeled as a porous medium with specific permeability and effective diffusivity. By extending the analytical solution to incorporate the stent layer, new species concentration distributions in the arterial layers are obtained in both the radial and the axial directions. The obtained analytical result clearly and readily shows the relationship between mass transport and LDL accumulation across the artery and permeability, porosity, length of the struts, reaction rate, etc. The impact of the stent compactness on the species transport within the arterial layers is investigated. The analytical solutions incorporating the presence of stent are compared with the numerical solutions and are found to be in good agreement.

References

[1] W. Rosamond, K. Flegal, G. Friday, et al., Heart disease and stroke statistics – 2007 update: a report from the American heart association statistics committee and stroke statistics subcommittee, Circulation 115 (2007) 69–171.
[2] D. Stoeckel, A. Pelton, T. Duerig, Self-expanding nitinol stents: material and design considerations, Eur. Radiol. 14 (2004) 292–301.
[3] N. Duraiswamy, R.T. Schoephoerster, M.R. Moreno, J.E. Moore Jr., Stented artery flow patterns and their effects on the artery wall, Annu. Rev. Fluid Mech. 39 (2007) 57–82.
[4] M. Prosi, P. Zunino, K. Perktold, A. Quarteroni, Mathematical and numerical models for transfer of low-density lipoproteins through the arterial walls: a new methodology for the model set up with applications to the study of disturbed luminal flow, J. Biomech. 38 (2005) 903–917.
[5] N. Yang, K. Vafai, Modeling of low-density lipoprotein (LDL) transport in the artery – effects of hypertension, J. Int. Heat Mass Transfer 49 (2006) 850–867.
[6] G. Rappitsch, K. Perktold, Pulsatile albumin transport in large arteries: a numerical simulation study, J. Biomech. Eng. 118 (1996) 511–519.
[7] S. Wada, T. Karino, Computational study on LDL transfer from flowing blood to arterial walls, in: T. Yamaguchi (Ed.), Clinical Applications of Computational Mechanics to the Cardiovascular System, Springer, Berlin, 2000, pp. 157–173.
[8] J.A. Moore, C.R. Ethier, Oxygen mass transfer calculations in large arteries, J. Biomech. Eng. 119 (1997) 469–475.
[9] D.K. Stangeby, C.R. Ethier, Coupled computational analysis of arterial LDL transport – effects of hypertension, Comput. Methods Biomech. Biomed. Eng. 5 (2002) 233–241.
[10] D.K. Stangeby, C.R. Ethier, Computational analysis of coupled blood-wall arterial LDL transport, J. Biomech. Eng. 124 (2002) 1–8.
[11] L. Ai, K. Vafai, A coupling model for macromolecule transport in a stenosed arterial wall, Int. J. Heat Mass Transfer 49 (2006) 1568–1591.
[12] M. Khakpour, K. Vafai, Critical assessment of arterial transport models, Int. J. Heat Mass Transfer 51 (2008) 80722.
[13] S. Chung, K. Vafai, Effect of the fluid-structure interactions on low-density lipoprotein within a multi-layered arterial wall, J. Biomech. 45 (2012) 371–381.
[14] K. Pannathai, K. Vafai, S. Phrut, T. Pradit, Effects of pressure on arterial failure, J. Biomech. 10 (2012) 1016.
[15] S. Chung, K. Vafai, Low-density lipoprotein transport within a multi-layered arterial wall-effect of the atherosclerotic plaque/stenosis, J. Biomech. 46 (2013) 574–585.
[16] L. Ai, K. Vafai, An investigation of Stokes' second problem for non-Newtonian fluids, Numer. Heat Transfer Part A 47 (2005) 955–980.
[17] N.A. Casson, Flow equation for the pigment oil suspensions of the printing ink type, Reology of Disperse Systems, Pergamon, New York, 1959.
[18] D. Quemada, A model for non-Newtonian shear viscosity in steady flows, Rheol. Acta 17 (1978) 632–642.
[19] M. Khakpour, K. Vafai, A comprehensive analytical solution of macromolecular transport within an artery, Int. J. Heat Mass Transfer 51 (2008) 2905–2913.

[20] C.C. Michel, F.E. Curry, Microvascular permeability, Physiol. Rev. 79 (1999) 703–761.
[21] J.M. Tarbell, Mass transport in arteries and the localization atherosclerosis, Annu. Rev. Biomed. Eng. 5 (2003) 79–118.
[22] K. Khanafer, R. Berguer, Fluid–structure interaction analysis of turbulent pulsatileflow within a layered aortic wall as related to aortic dissection, J. Biomech. 42 (2009) 2642–2648.
[23] J.P. Abraham, J.M. Gorman, E.M. Sparrow, J.R. Stark, R.E. Kohler, A mass transfer model of temporal drug deposition in artery walls, Int. J. Heat Mass Transfer 58 (2013) 632–638.
[24] N. Yang, K. Vafai, Low-density lipoprotein (LDL) transport in an artery – a simplified analytical solution, J. Int. Heat Mass Transfer. 51 (2008) 497–505.
[25] L. Ai, K. Vafai, A coupling model for macromolecule transport in a stenosed arterial wall, Int. J. Heat Mass Transfer 49 (2006) 1568–1591.
[26] G. Meyer, R. Merval, A. Tedgui, Effects of pressure stretch and convection on low-density lipoprotein and albumin uptake in the rabbit aortic wall, Circ. Res. 79 (3) (1996) 532–540.
[27] G. Pontrelli, F. de Monte, A multi-layer porous wall model for coronary drug-eluting stents, Int. J. Heat Mass Transfer 53 (2010) 3629–3637.
[28] G. Pontrelli, F. de Monte, Modeling of mass dynamics in arterial drug-eluting stents, J. Porous Media 12 (2009) 19–28.
[29] F. Migliavacca, F. Gervaso, M. Prosi, P. Zunino, S. Minisini, L. Formaggia, G. Dubini, Expansion and drug elution model of a coronary stent, Comput. Methods Biomech. Biomed. Eng. 10 (2007) 63–73.